Quantifying the impacts of large-scale implementation of white roofs on the climate of Montreal Island through integrated super-resolution modeling

Results in Engineering 28 (2025) 107572

Contents lists available at ScienceDirect

Results in Engineering

journal homepage: www.sciencedirect.com/journal/results-in-engineering

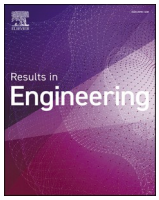

Research paper

Quantifying the impacts of large-scale implementation of white roofs on the climate of Montreal Island through integrated super-resolution modeling

Shinto Roose *, Laxmi Sushama

Department of Civil Engineering and Trottier Institute for Sustainability in Engineering and Design, McGill University, Montreal, Canada

ARTICLE INFO

Keywords:
Urban heat mitigation
White roofs
Super-resolution climate simulation

ABSTRACT

The net impact of large-scale implementation of white roofs, one of the many urban heat mitigation strategies widely being adopted, on the urban climate is investigated. This is achieved through super-resolution (250 m) regional climate model simulations, with and without white roofs, for summer, for the island of Montreal, Canada. Being surrounded by water bodies, local winds such as land and sea breezes are important for the island, which are captured by the super-resolution climate simulation along with other climate characteristics. Grid-averaged surface and 2 m temperature results suggest general cooling with white roof implementation. However, analysis shows warming for the non-urban fractions in different parts of the island as a result of the complex interactions between various aspects of the regional climate system. During daytime, this warming, particularly noted for the west and central parts of the island, is associated with reduced latent heat flux in the white roof simulation, caused by reduced surface energy, weakening of sea breeze circulation, and decreased soil moisture from reduced convective precipitation. During nighttime, the white roof enhanced land breeze also warms the non-urban fractions of low-density urban zones in the eastern and western parts of the island, through advection of relatively warmer air from nearby urban areas. The new insights on the adverse effect of large-scale white roof implementation, primarily triggered by changes in local/non-synoptic winds, highlight the need for integrated modelling in quantifying the net impact of urban heat mitigation strategies, which is crucial for providing equitable benefits to all regions.

1. Introduction

Urban regions worldwide are grappling with the dual challenges of climate warming driven by greenhouse gas emissions [1] and the urban heat island effect (UHI). UHI results from a combination of factors, including the heat-absorbing properties of urban building and pavement materials, additional anthropogenic heat sources, the trapping of long-wave radiation within the urban canopy, reduced ventilation, reduced wind speed due to urban surface roughness, reduced evapotranspiration, and consequently reduced evaporative cooling [2,3]. Over half of the world's population now resides in urban regions, with around 80 % of the population in high-income countries residing in highly urbanized areas as urbanization continues to change the landscape [1,4]. By 2050, almost 70 % of the world's population is expected to live in urban areas [5,6], which can further exacerbate UHI, energy demands for cooling and impacts on public health, air quality, and overall urban livability [7].

Extensive research has been conducted to investigate UHI across various climatic zones, utilizing both numerical modeling and observational methods [8–11]. Recent interest has been in quantifying the impacts of various heat mitigation strategies. These strategies include urban greening initiatives, such as urban forests and green roofs, which enhance shading and evaporative cooling [12–18], and increasing urban surface albedo through reflective pavements and white roofs, amongst others [19–26]. White/cool roofs have emerged as a popular approach for mitigating the UHI effect, given space limitations in the urban regions for other strategies such as urban forests, and availability of large number of rooftops. The geographic characteristics and urban-climate interactions can influence significantly the cooling performance of white roofs. White roofs have a more efficient cooling impact when they are situated in areas with higher solar radiation, less precipitation, weak winds, and when roofs have lower water-holding capacity (i.e., when they quickly dry or drain rainwater), and lower thermal admittance [27].

Standalone urban models are generally used to demonstrate the utility of heat mitigation strategies. For instance, Kaloustian et al. [28]

* Corresponding author.
E-mail address: shinto.roose@mcgill.ca (S. Roose).

https://doi.org/10.1016/j.rineng.2025.107572
Received 7 August 2025; Received in revised form 21 September 2025; Accepted 3 October 2025
Available online 3 October 2025

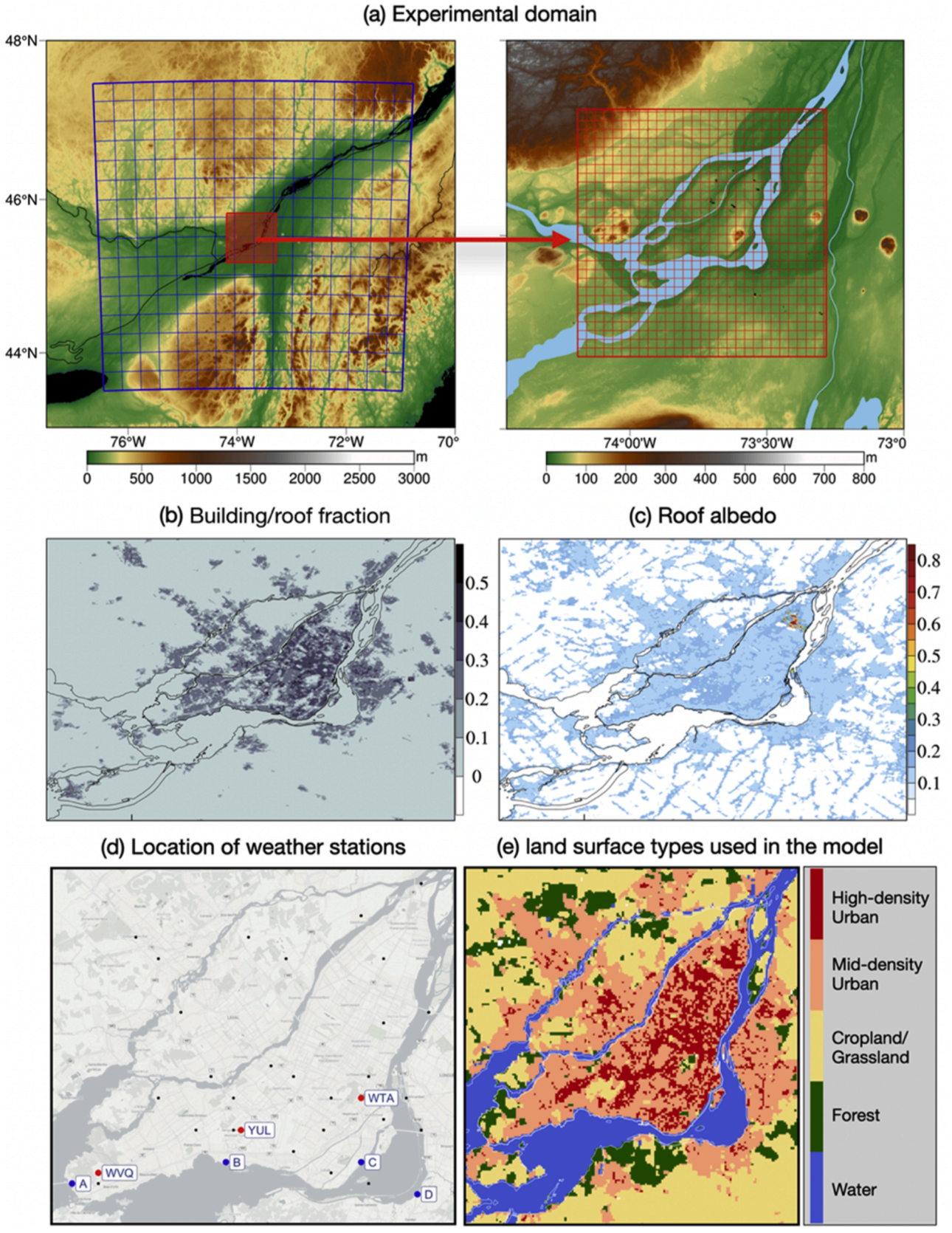

Fig. 1. (a) GEM domain at 2.5 km resolution, with blue lines showing every 10th grid cell and GEM experimental domain at 250 m resolution, with red lines showing every 10th grid cell. The colour represents topography, with water bodies depicted in light blue. (b) Building/roof fraction, and (c) roof albedo in GEM_REF simulation. (d) Geographical distribution of meteorological stations within the study domain (red filled circles), with those considered in this study shown in red. A-D are additional points considered for analysis. (e) Land cover at 250 m resolution.

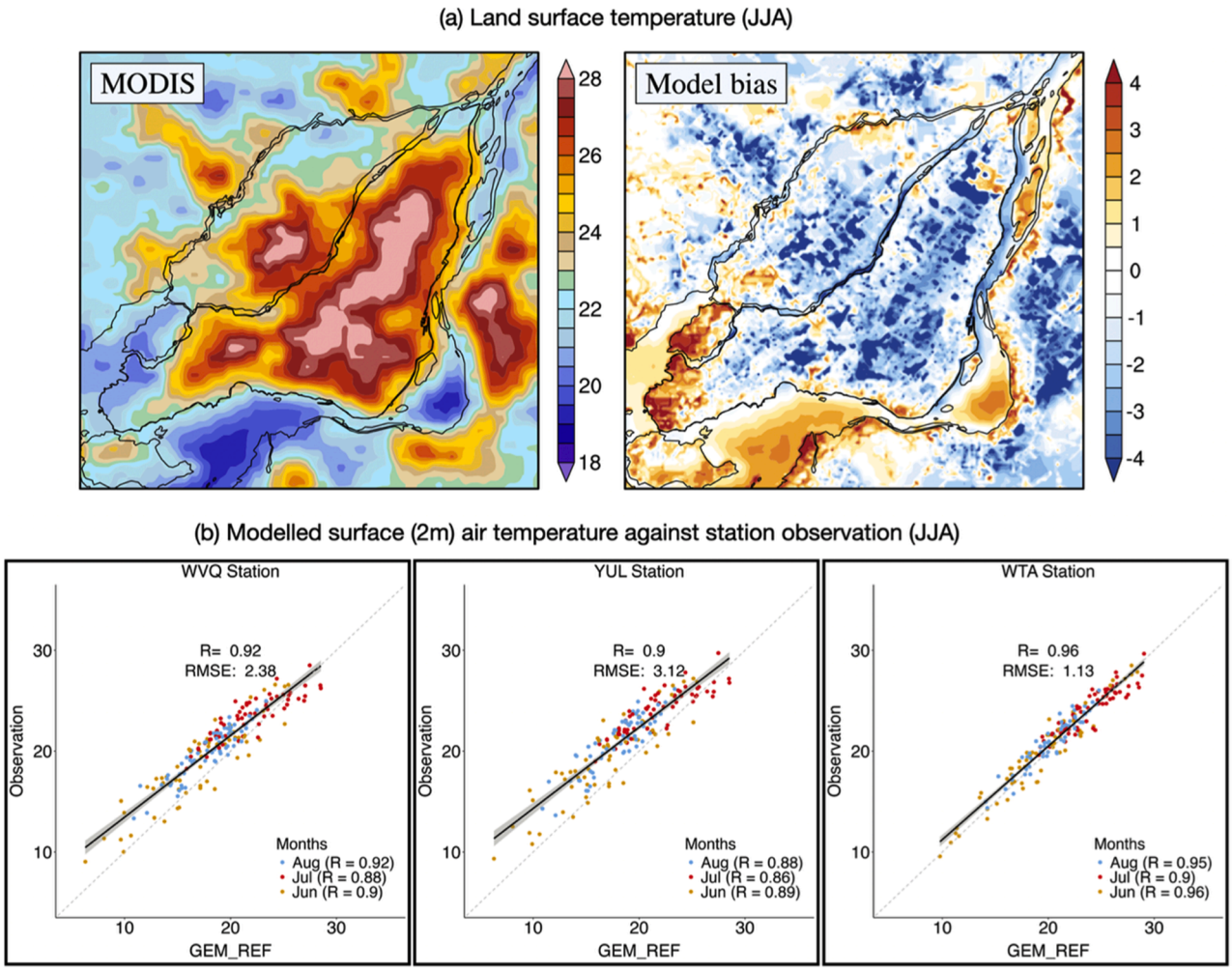

Fig. 2. (a) MODIS-based mean summer land surface temperatures (°C) and GEM_REF biases with respect to MODIS. (b) Scatter plots comparing 2 m air temperatures (°C) from GEM_REF with those at observation stations. The fitted linear regression line and correlation coefficient (R) indicate the association between the two datasets; the grey shading represents the 95 % confidence interval, and the dashed line indicates the identity line (1:1 line).

used the town energy balance (TEB) model to study the impact of high albedo pavements and roofs in mitigating UHI. However, such stand-alone or offline simulations cannot capture urban-atmosphere interactions and feedback, which are crucial for comprehensive assessment of the effectiveness of these mitigation strategies. Climate models with improved representation of urban regions are required to realistically simulate these feedbacks and interactions. Urban regions are not adequately represented in many climate models primarily due to their coarse resolution. However, with advances in computing resources, high-resolution Regional Climate Model (RCM) simulations are becoming more feasible. These simulations can incorporate improved parameterizations specifically for urban fractions, which can help to better understand urban-atmosphere interactions and feedback (e.g., [29–31]).

RCMs with urban regions represented using urban canopy models have been used in some recent studies to evaluate the cooling potential of heat mitigation techniques, offering valuable insights [32–36]. Such studies are limited for water-bound cities, like Montreal, which is the second largest urban center in Canada, where land and sea breezes can modulate regional climate. This study aims at understanding the net benefits of white roofs as a heat mitigation strategy for the island of Montreal through super-resolution RCM simulations. Such high-resolution simulations are critical for resolving regional characteristics such as local wind circulation patterns, including land and sea breezes, and associated direct and indirect responses for better comprehension of the net climatic benefits of reflective roofing. As Montreal continues to grow and evolve, assessing the effectiveness of heat mitigation strategies will be crucial for informing sustainable urban planning and public health initiatives. It can also contribute to the broader understanding of urban climate dynamics, which will ultimately enhance the city's resilience and livability for its residents.

The rest of the paper is organized as follows. Section 2 provides comprehensive details on the model, datasets, and methodology used in the analysis. Section 3 delves into the results, encompassing the findings related to temperature changes and wind patterns influenced by the heat mitigation strategy considered in the study. Finally, Section 4 summarizes the key conclusions and implications of the study, highlighting potential areas for future research.

2. Model and methods

Using an integrated approach, this study aims to assess the net benefits of white roof as a heat mitigation strategy, with Montreal as the case study. Being an island, local wind patterns, i.e., non-synoptic winds, driven by land-water thermal/pressure gradients modulate the urban heat characteristics. Such land-sea breeze-type pattern may contribute to heat modulation in urban areas, and the effect could be more pronounced for shoreline regions. These local circulations, despite being less pronounced than their counterparts in oceanic settings, can still be influential. The combined effect of these non-synoptic winds and white

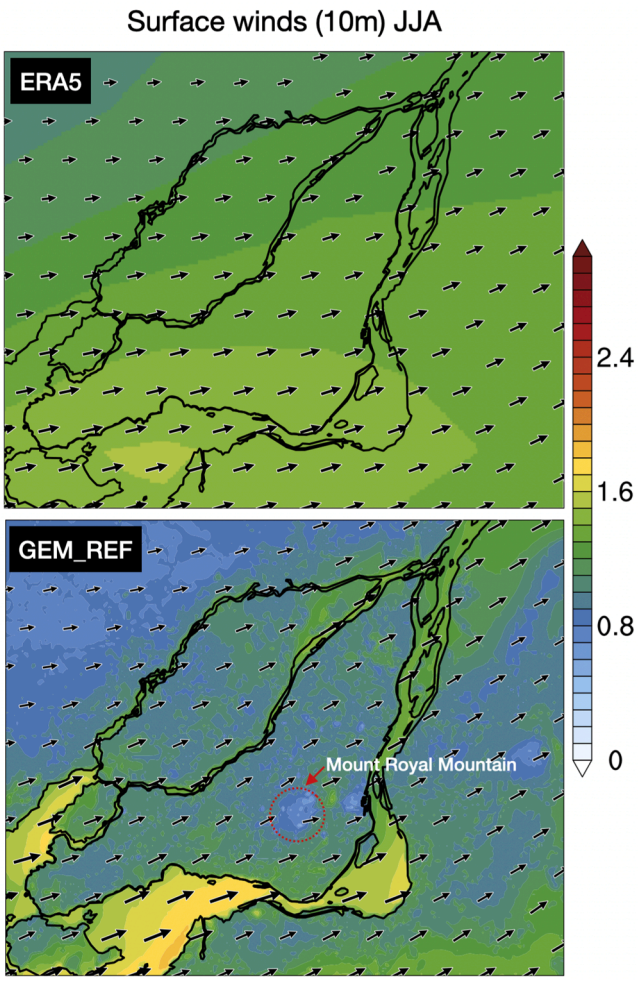

Fig. 3. Mean summer 10 m winds (in ms^{-1}) from ERA5-land and GEM_REF for 2019 and 2020.

roofs on the urban heat characteristics and the local climate in general have not been adequately explored. This is critical in understanding the net benefit of the heat mitigation strategy.

Two RCM simulations, with and without white roof, performed with the Global Environmental Multiscale (GEM; [37]) model, are employed to understand the impact of large-scale implementation of white roofs on the linkage between local wind patterns and urban heat and precipitation characteristics. These simulations are performed at a horizontal grid resolution of 250 m, driven at the lateral boundaries by a GEM simulation at ~2.5 km resolution, which in turn is driven by the European Centre for Medium-Range Weather Forecasts (ECMWF) fifth-generation reanalysis product, ERA5 [38]. The GEM experimental domain covering Montreal comprises of 324 × 324 grid points (Fig. 1a). The model solves non-hydrostatic, deep atmosphere dynamics with implicit, two-time-level semi-Lagrangian numerical scheme. The scheme employed for condensation processes is the double-moment microphysics scheme of Milbrandt & Yau [39]. Radiation is parametrized by Correlated K solar and terrestrial radiation [40]. The planetary boundary layer scheme follows Benoit et al. [41] and Delage [42], with some modifications, as described in Zadra et al. [43]. A detailed description of the model and its parameterization schemes are given in Diro and Sushama [44]. The land part in GEM is represented by the Canadian Land Surface Scheme (CLASS), which allows flexible soil layer configuration [45]. CLASS provides a physically based framework for energy, momentum, and water exchanges between the land surface, vegetation canopy, and the atmosphere.

The urban fractions in the model are represented by TEB [46] scheme, which accounts for the urban energy budget based on a generalization of local canyon geometry. Buildings are assumed to be located along identical roads leading to the canyon structure. The lengths of the roads are considered to be far greater than their widths, and the buildings bordering the street canyon are assumed to have the same height and width within a model grid cell. In TEB, the urban morphology for each grid cell is defined in terms of the building and road fractions, building height, building and canyon aspect ratio, and roughness length. The radiative characteristics such as albedos and emissivity for roofs, roads, and walls and thermal properties such as thermal conductivity and heat capacity of each roof, road, and wall layer are prescribed. Fig. 1b illustrates the building/roof fractions over the experimental domain, with a notably higher density over Montreal Island. The 250 m resolution enables better representation of surface heterogeneity, land-water demarcation, and urban morphology, all of which strongly influence local circulation patterns. Furthermore, the coupled system enables realistic simulation and therefore realistic quantification of the net effect of the urban heat mitigation strategy considered in the study.

The two GEM simulations, i.e., the control simulation (GEM_REF) and the white roof simulation (GEM_WR), span the April 1 to August 31 period of 2019 and 2020. Although simulations span the April to August period, analysis considered in this study focusses on the summer (June–August) period, when the UHI effect is most noticeable, and the potential benefits of white roofs are most obvious. The study was restricted to 2019 and 2020 due to the computationally expensive nature of the super-resolution simulations. White roof is represented in GEM_WR in terms of high roof albedos. In GEM_REF, the albedo values for roofs for most of the urban region are generally <0.2, except for a region – the Montreal Refinery area in northeast Montreal (Fig. 1c) – that employ white oil storage tanks. An albedo value of 0.8 is prescribed for roofs in the white roof experiment, GEM_WR.

Model validation is first performed by comparing GEM_REF against available observations. This is an important step prior to undertaking the mitigation experiment to confirm GEM's ability in realistically simulating the urban climate. Given the interest in urban heat modulations, the variables validated are land surface temperature, 2 m air temperatures, surface (10 m) winds and precipitation. Hourly observed temperature and wind data at selected locations from Environment and Climate Change Canada (ECCC) are utilized to validate GEM simulated fields. Out of the 37 observation stations in the study domain, three of them, namely Ste-Anne-De-Bellevue (WVQ), Pierre Elliot Trudeau Intl (YUL), and McTavish (WTA) (Fig. 1d) are selected for validation as they provide continuous records for the study period, enabling a detailed analysis of local weather patterns. Furthermore, the selected stations reflect a range of urban environments: BVQ is located in a highly vegetated region of Montreal Island, YUL is situated at the airport site representing a more open environment, and WTA is located in a high urban density region. Additionally, gridded estimates of surface temperature and precipitation from Daymet data [47], which is available at 1 km spatial resolution and daily temporal resolution, is also considered for validation. Daymet is obtained by interpolating and extrapolating ground-based observations through statistical modeling techniques, along with bias corrections. As Daymet does not explicitly account for urban morphology, it has limitations when applied to heterogeneous urban regions; nevertheless, it provides valuable large-scale coverage for model evaluation. In order to determine whether the overall magnitude and patterns of modeled surface winds are appropriately represented, winds at 10 m are verified against the ERA5-land reanalysis [48], despite its ~9 km spatial resolution. Additionally, satellite-based land surface temperature data from Moderate Resolution Imaging Spectroradiometer (MODIS) is also used. This data is available at a spatial resolution of 1 km, twice a day (10:30 and 22:30 local solar time (LST)). The MODIS data is bilinearly interpolated to match the model grid for validation purposes.

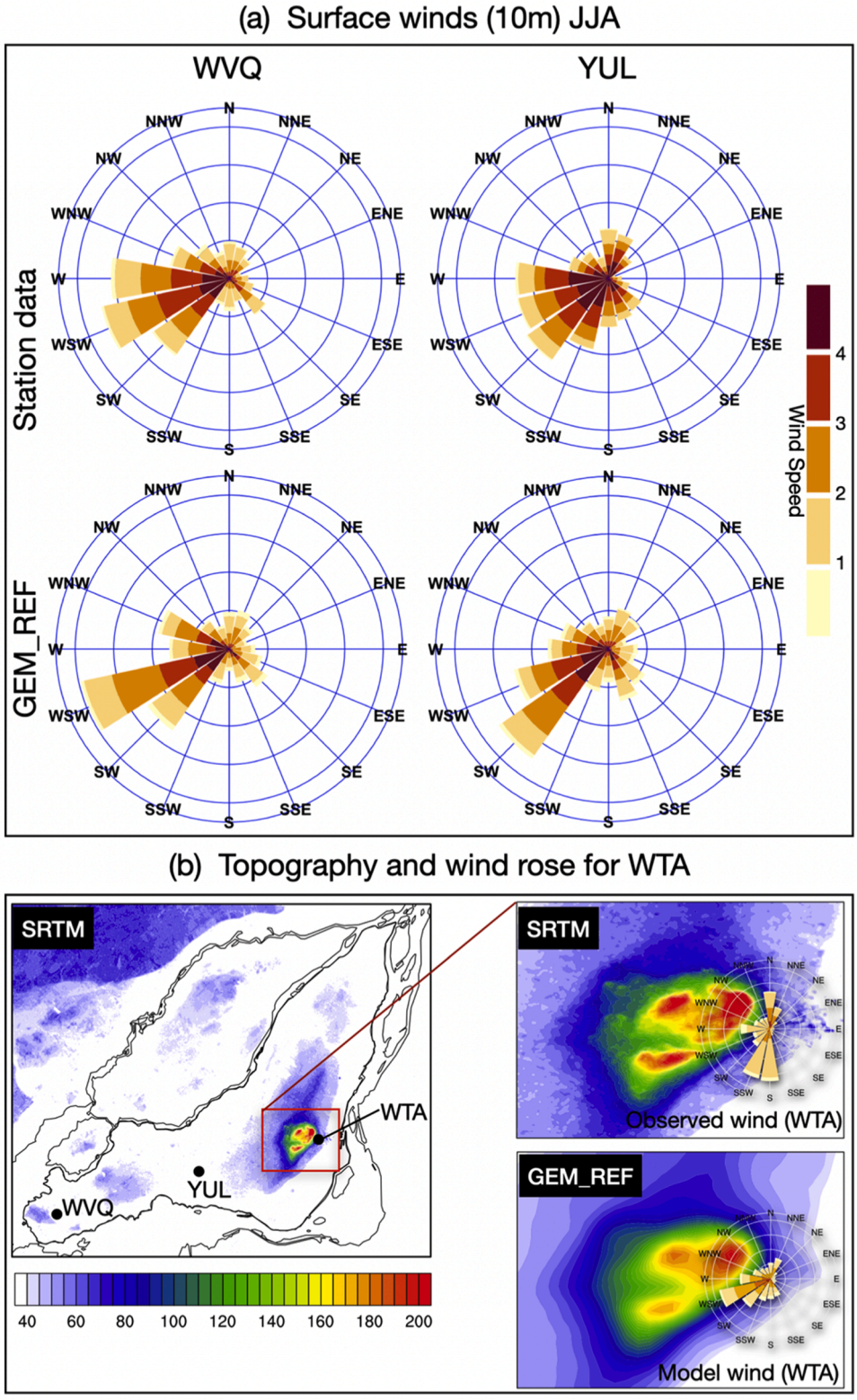

Fig. 4. (a) Wind rose diagrams for observed and GEM_REF modelled winds (ms^{-1}) at stations WVQ (left) and YUL (right) for summer for years 2019 and 2020. (b) (Left) Topography (m) from the Shuttle Radar Topography Mission (SRTM) and GEM model. (Right) Wind rose diagram for the observed and GEM_REF winds at the WTA station are also shown.

3. Results

3.1. Model validation

Validation of GEM_REF simulated land surface and 2 m temperatures, wind and precipitation characteristics, by comparing with respective observations as indicated in Section 2, are presented here. The MODIS-based mean summer land surface temperature clearly indicates the UHI over Montreal Island (Fig. 2a), with warmer temperatures for the high-density urban regions in the central part of the island,

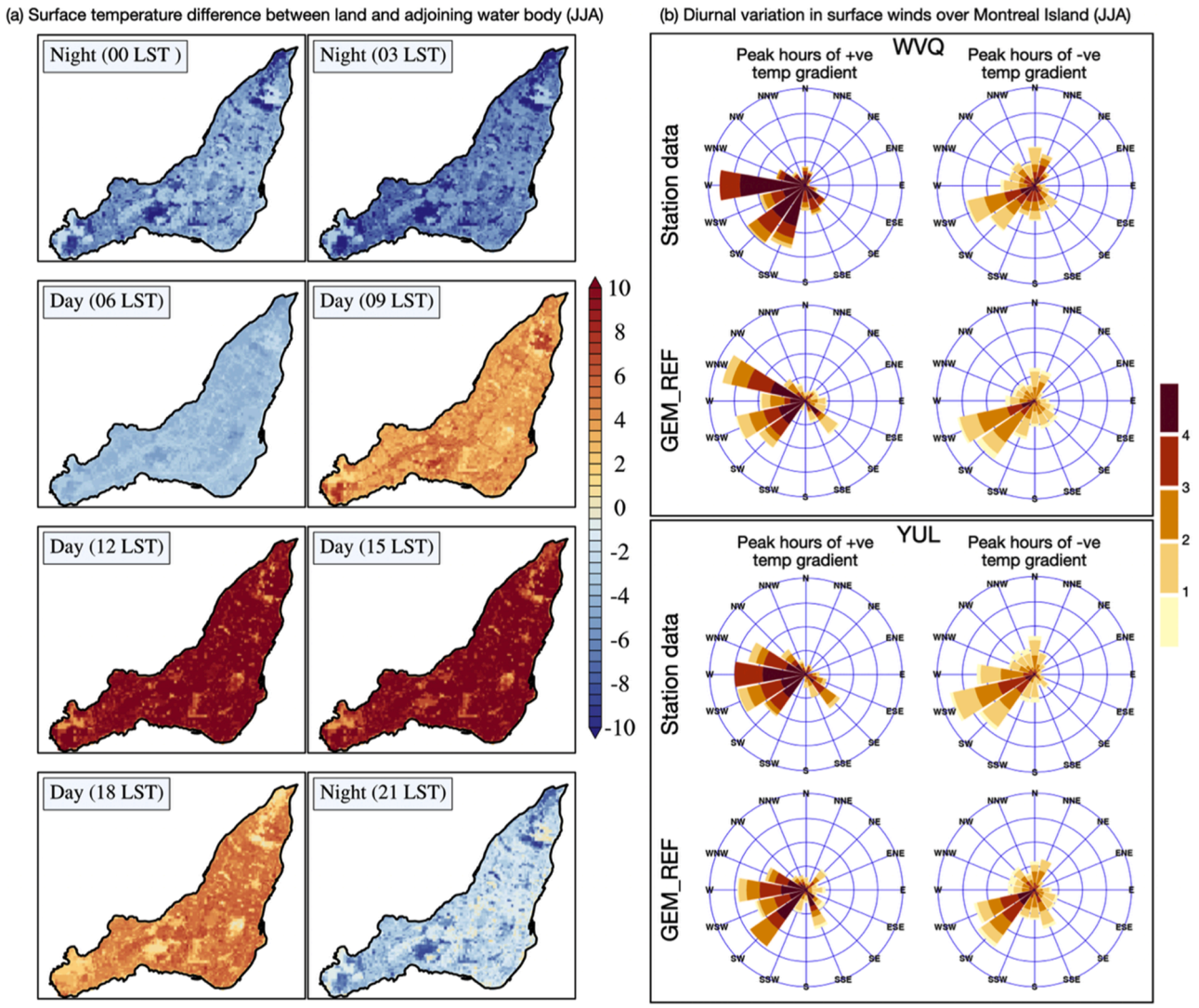

Fig. 5. (a) Mean surface temperature (°C) differences between land and surrounding water. (b) Wind rose diagrams for peak hours of +ve (left) and -ve (right) temperature gradients, for GEM_REF and station observations (WVQ and YUL) for summer for years 2019 and 2020.

i.e., the urban core, and cooler temperatures elsewhere. Comparison of GEM_REF simulated LST with MODIS (Fig. 2a) indicates warm biases for certain regions of Montreal, particularly the western tip of the island with high vegetation fraction, while cold biases are noted over neighbouring grid cells of high-density urban regions. It must however be noted that the accuracy of satellite-based land surface temperature measurements is often constrained by the complexity of land surface types (Sun et al., 2004; [49]), and therefore may have deficiencies. Furthermore, the low resolution (1 km) of MODIS data compared to the model resolution of 250 m will also have difficulties in capturing the high-resolution information. Considering all these factors, it seems that the modelled land surface temperature is reasonable.

In a recent study by Vincent and Sushama [50] using an offline simulation with CLASS and TEB, using the same grid configuration and resolution as in this study, significant warm biases along the shoreline regions of Montreal were reported. They attributed these biases to the lack of land-atmospheric coupling and therefore shoreline wind patterns which have the ability to cool regions adjoining water bodies during warmer periods of the day in the form of sea breeze. The coupled configuration/model used in this study has significantly improved the shoreline land surface temperature for the Montreal Island, resulting in almost close to zero biases mostly.

Comparison of 2 m air temperatures at three observation sites with the most representative grid cells suggests that the model effectively captures the temporal variations during summer (Fig. 2c), with a correlation coefficient (R) ranging from 0.9 to 0.96. Daily temperature values for each of the three summer months separately show a strong correlation with observations, indicating that the model effectively captures intraseasonal temperature variations during summer. These results suggest that the GEM model adequately captures the 2-meter summer air temperature characteristics.

Fig. 3 presents the spatial pattern of mean summer wind speed and direction from ERA5-land and GEM_REF for 2019 and 2020. Although ERA5-land has a significantly coarser resolution than that of the GEM simulation, it provides critical insights into the large-scale surface wind dynamics. Analysis of ERA5-land suggests that the surface winds are predominantly southwesterly, which is captured by the model. The wind pattern is more uniform in ERA5-land, while it is more realistic in GEM_REF due to the very high resolution which captures the impact of surface characteristics/types, such as higher wind magnitudes over the waterbody due to low surface roughness, and similarly realistic wind trajectories near regions with important topography such as the Mount Royal Mountain in the south central part of the island.

To further support validation, GEM_REF-based wind roses are compared with those at observation stations. Comparison of summer wind roses for 2019 and 2020 suggests that the overall patterns and

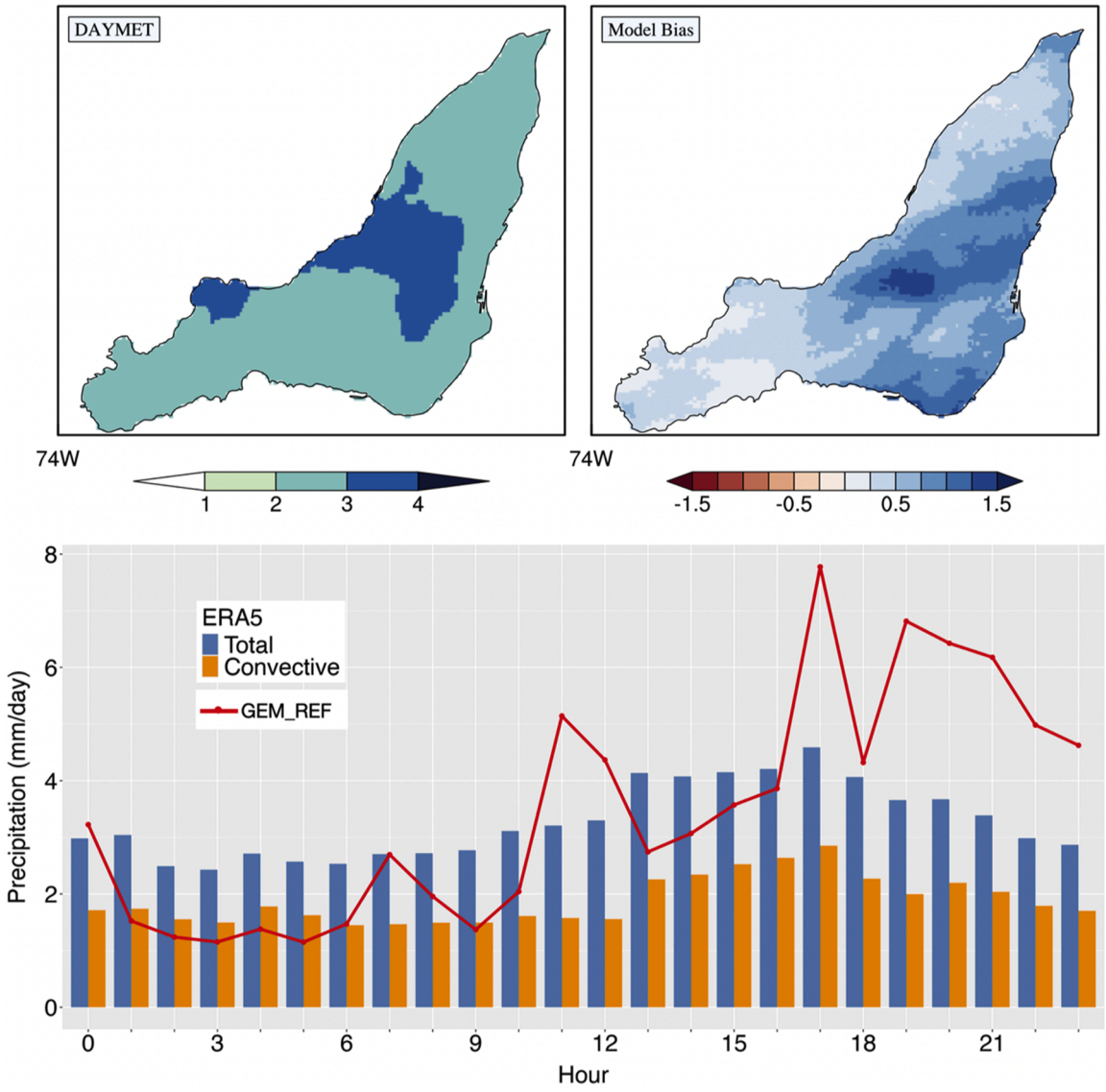

Fig. 6. Mean summer precipitation (in mm/day) for years 2019 and 2020 from Daymet (top left), and GEM_REF biases compared to Daymet (top right). Diurnal variation of summer precipitation over Montreal from GEM_REF and ERA5 (bottom); the contribution of convective precipitation is also shown for ERA5.

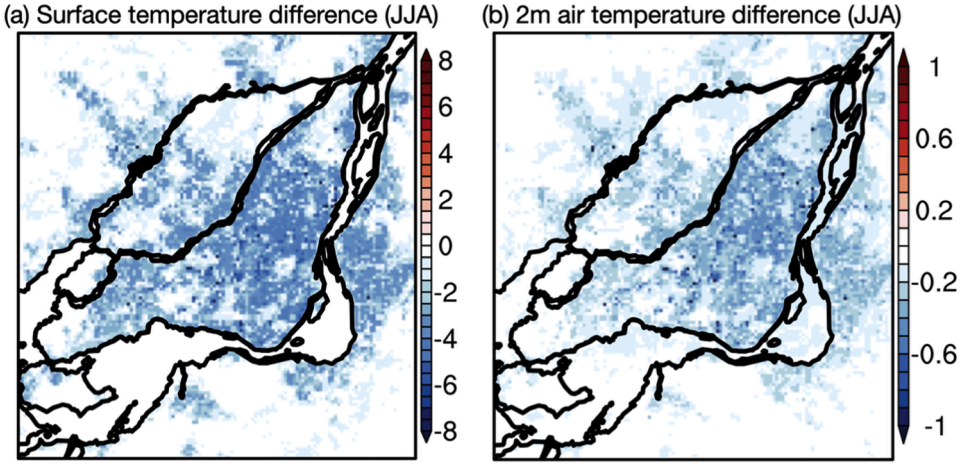

Fig. 7. (a) Surface temperature (°C) and (b) 2 m air temperature (°C) differences between GEM_WR and GEM_REF simulations during summers of 2019 and 2020.

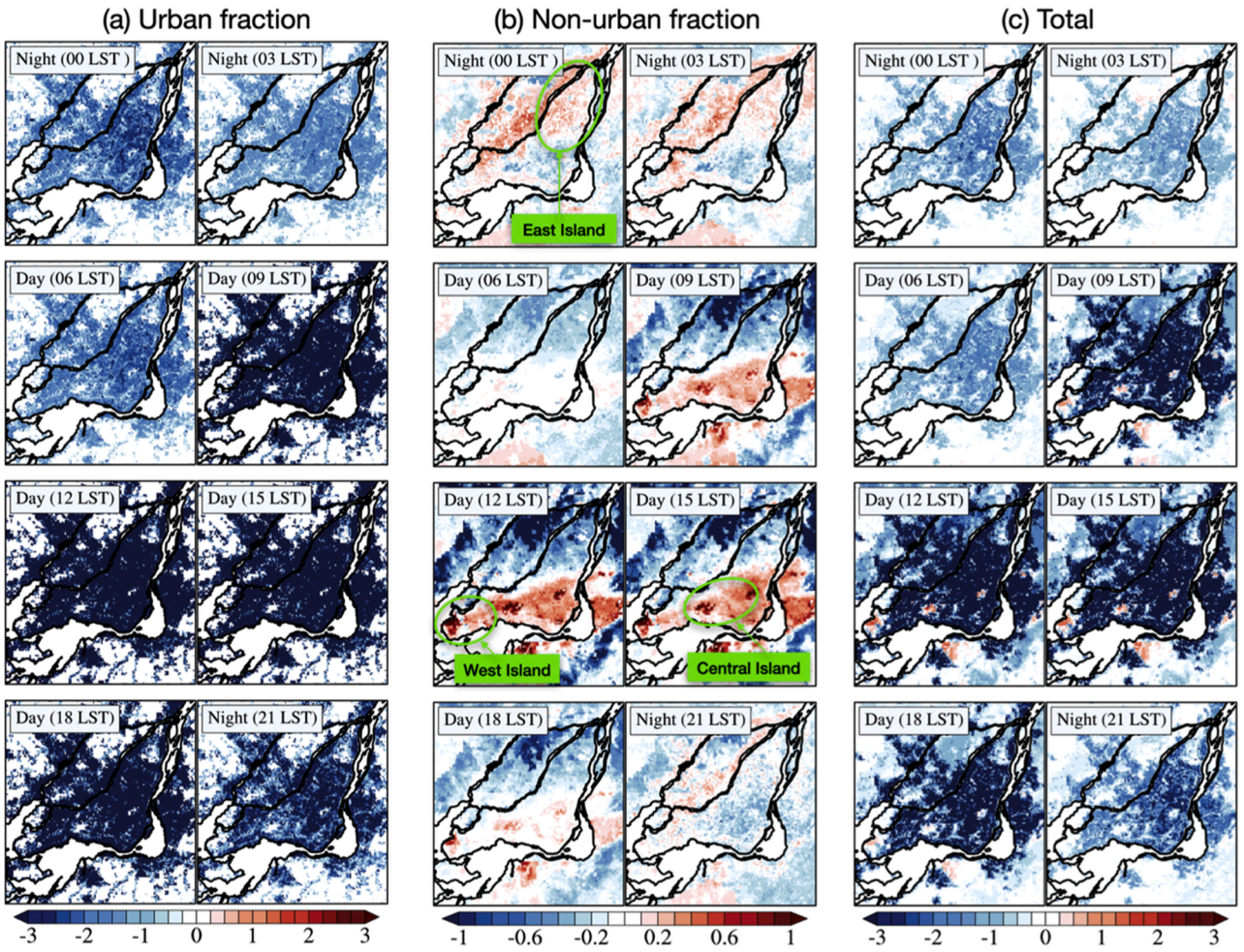

Fig. 8. Mean summer surface temperature (°C) differences between GEM_WR and GEM_REF for years 2019 and 2020, for the (a) urban and (b) non-urban fractions of grid cells, and (c) for the entire grid cell.

intensity of surface winds at 10 m are captured for the WVQ and YUL stations (Fig. 4a). Similar to the observed wind roses, the modelled pattern at these stations demonstrates that strong winds predominantly come from the west to southwest directions. The third station, McTavish (WTA), located along the slopes of the Mount Royal Mountain in the centre of the island of Montreal, presents unique challenges. The 250 m resolution seems still inadequate in realistically representing the complex topography and wind patterns associated with this region. For example, comparison of the topography in the model with that from the Shuttle Radar Topography Mission (SRTM) shown in Fig. 4b reveals significant differences, especially for the high elevation regions. This observation underscores the importance of spatial resolution in accurately depicting topographic features. Consequently, such disparities introduce biases in wind. At WTA, the modeled winds are dominated by west-southwesterlies; however, these winds are not predominant in the observed data because the high terrain to the west-southwest of the WTA station obstructs wind flow toward the station. Despite this difference, the overall patterns and intensity of surface winds seem reasonable for the rest of the island of Montreal.

The model ability in capturing land-sea breeze type wind is also analysed. The occurrences of these are governed by land-water temperature differences, caused by their different heat capacities, the diurnal pattern of which is shown in Fig. 5a for GEM_REF. Given the relatively small spatial variation in surface temperature for the water bodies surrounding the island, the temperature difference for each land grid point is estimated as the difference between the surface temperature for the land point and the average value for the water bodies. The maximum positive temperature gradient is noted (Fig. 5a) at around 15 LST, while the maximum negative gradient is noted at 03 LST. Based on the peak hours of land-water temperature gradient, wind roses for these and adjoining hours (i.e., 13–16 LST and 21–04 LST) from GEM_REF are compared to those observed at WVQ and YUL (Fig. 5b) to assess model ability in simulating daytime sea breeze and nighttime land breeze, respectively.

Wind roses at both stations depict predominantly west-northwesterly to southwesterly winds for the time periods selected (Fig. 5b). These intensify during periods of maximum positive temperature gradient (13–16 LST) due to sea breeze. These winds significantly weaken during night hours as the land-water temperature gradient reverses. During the maximum negative temperature gradient hours, northwesterly to north-northeasterly winds are observed at both stations, which signify land breeze. GEM_REF-based wind roses also indicate the presence of these non-synoptic wind patterns, although with some underestimation. Fig. S1 (supplementary material) further demonstrates similar land-sea breeze features in the simulation (GEM_REF) for other shoreline locations marked in Fig. 1d. Wind rose diagrams are superimposed on a geographic map for better interpretation/comprehension of wind direction related to land/sea breezes. The figure further supports that the high-resolution of the model is able to represent reasonably well the dynamics of land/sea breezes.

The model simulation also shows good representation of summer mean precipitation pattern when validated against Daymet observation (Fig. 6). As in the Daymet observation, modeled precipitation maximum is over the high-density urban region, albeit with some overestimation

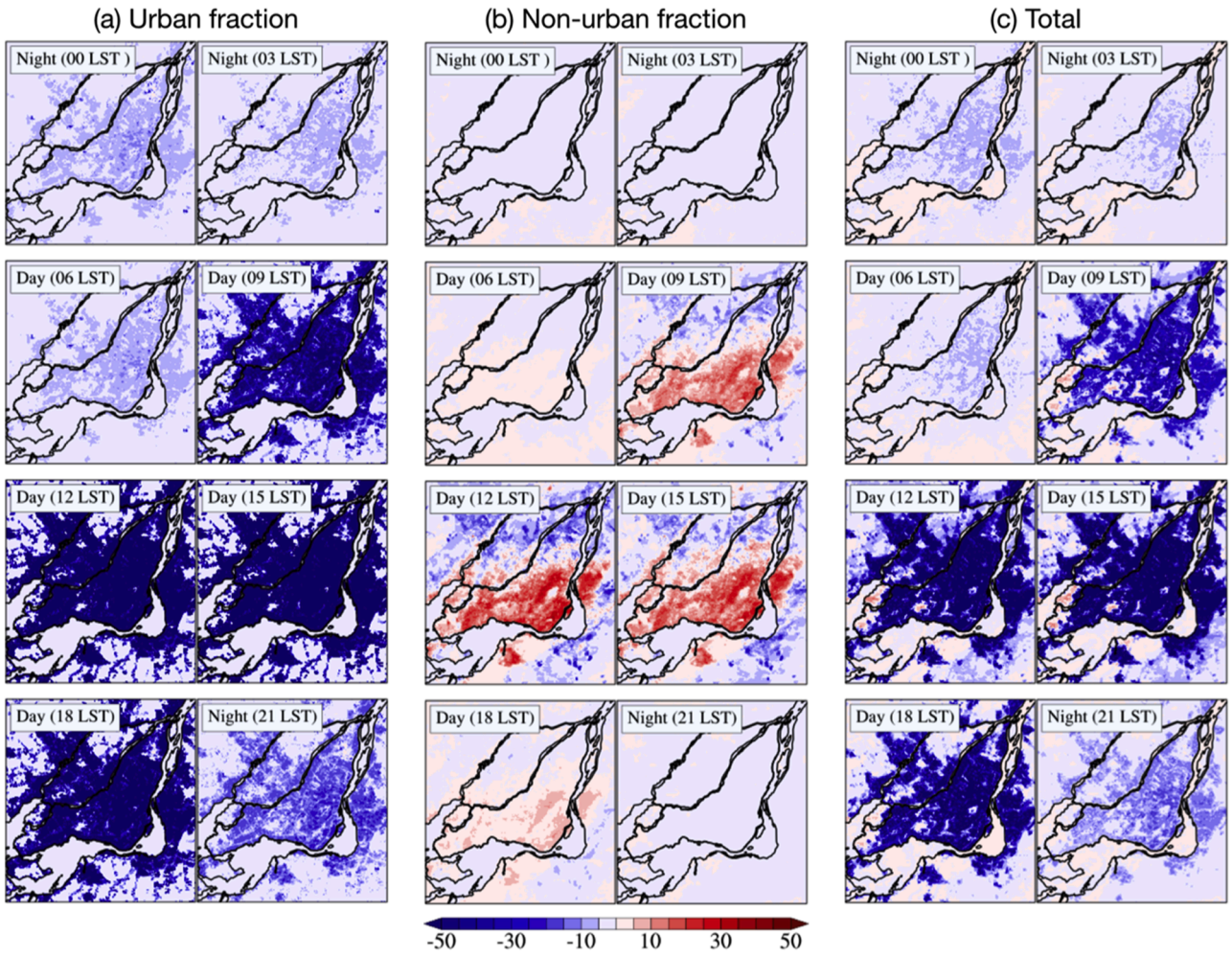

Fig. 9. Mean summer sensible heat flux (Wm^{-2}) differences between GEM_WR and GEM_REF simulations for years 2019 and 2020, for the (a) urban and (b) non-urban fractions of grid cells, and (c) for the entire grid cell.

ranging from 0 to 1.5 mm/day. Analysis of the diurnal pattern in GEM_REF (Fig. 6; bottom panel) shows that precipitation over the island of Montreal mostly occur in the evening hours (16–20 LST) during summer, with intense precipitation mostly occurring around 17 LST. This is also reflected in ERA5-based precipitation, which additionally confirms that precipitation for the evening hours is predominantly convective in nature for the studied period.

The ability of the model in capturing reasonably well the surface air temperature, mean and non-synoptic surface winds and precipitation spatiotemporal characteristics as demonstrated above and summarized in Table S1 gives confidence in conducting the planned experiment using GEM.

3.2. Urban climate-white roof interactions

The impact of white roof implementation on the urban climate is assessed by comparing GEM simulations with (GEM_WR) and without (GEM_REF) white roof. Fig. 7 shows the differences in mean summer surface temperature and 2 m air temperatures between GEM_WR and GEM_REF across the experimental domain (Fig. 7b). Clearly, GEM_WR has cooler temperatures, with cooling more noticeable for the high-density urban regions, with values up to 6.18°C (0.44°C) for surface (2 m) temperature. However, analysis of differences in surface and 2 m temperatures between the two simulations for urban and non-urban fractions reveal interesting results, which have huge implications from UHI mitigation and thermal comfort perspectives, which are discussed here.

Fig. 8 shows spatial patterns of mean summer surface temperature differences between GEM_WR and GEM_REF for selected hours of the day. Based on the diurnal evolution of net shortwave radiation, daytime will be considered as 05:00 to 20:00 LST, and nighttime as 21:00 to 04:00 LST for discussions and analysis to follow. As expected, cooling is more pronounced for the urban fractions (Fig. 8a) compared to non-urban fractions (Fig. 8b) for all times considered. The non-urban fractions show complex patterns, indicating many mechanisms at play. During daytime, surface temperatures for non-urban fractions are generally higher over Montreal in GEM_WR compared to GEM_REF, except for the eastern region of the island. During nighttime, there is a reversal, with cooler surface temperatures in GEM_WR for southern regions and higher temperatures to the east and west of the island. The 2 m temperature also reflects patterns similar to the surface temperature for both urban and non-urban fractions (Fig. S2). However, the differences for non-urban fractions are generally smaller than that for urban fractions. To understand the spatial patterns of the differences for non-urban fractions, differences in sensible and latent heat fluxes, between the two simulations (Fig. 9), for the same times as in Fig. 8, are analyzed. The lower temperatures in GEM_WR for the urban fractions, is primarily and directly related to the higher roof albedo values leading to less solar radiation absorbed at the surface and therefore reduced sensible heat fluxes (Fig. 9). Although decreases are noted in latent heat fluxes as well in GEM_WR compared to GEM_REF (Fig. 10), which could contribute to increasing surface temperature, these differences are much smaller

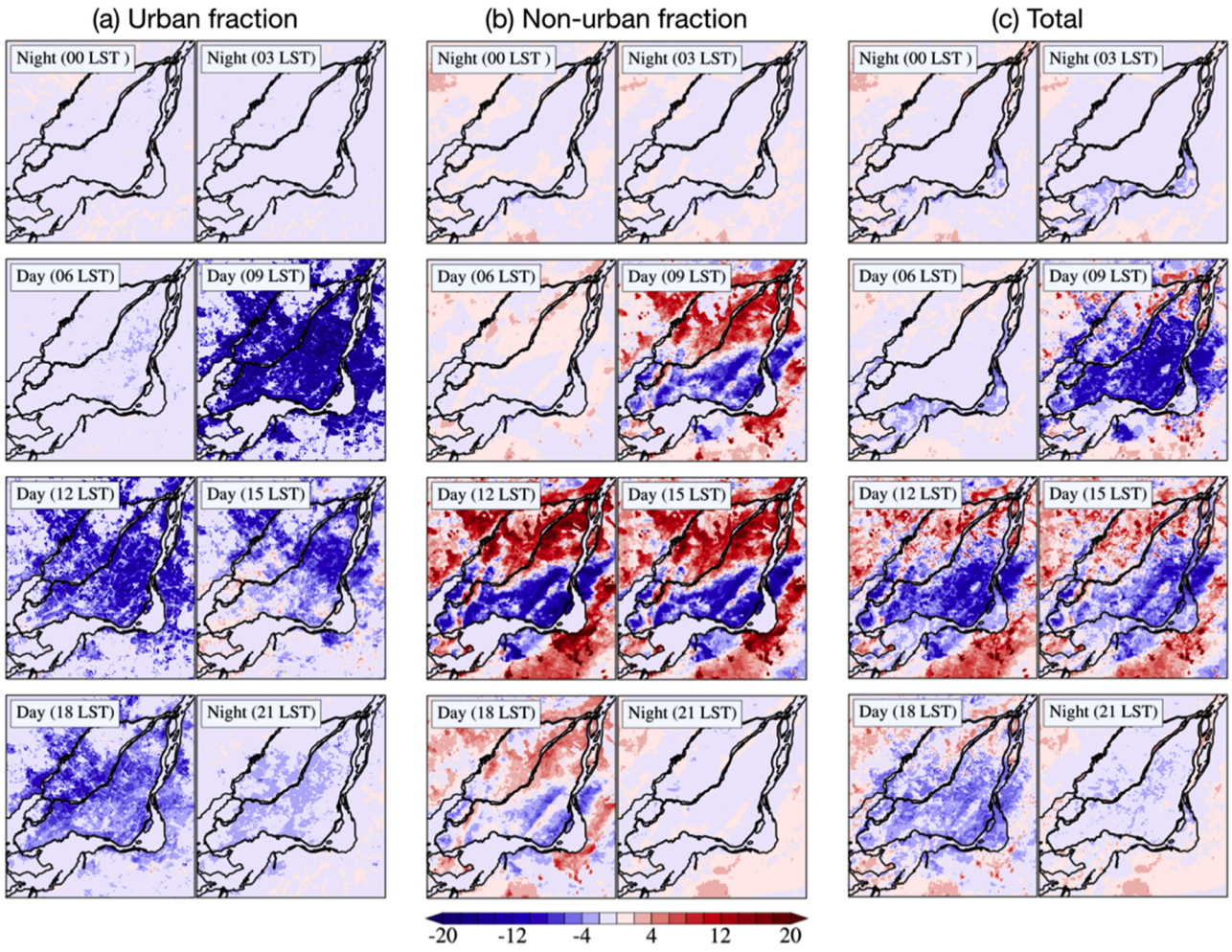

Fig. 10. Mean summer latent heat flux (Wm^{-2}) differences between GEM_WR and GEM_REF simulations for years 2019 and 2020, for the (a) urban and (b) non-urban fractions of grid cells, and (c) for the entire grid cell.

compared to that for sensible heat fluxes.

As for non-urban regions, the temperature difference patterns match those for the latent heat flux and sensible heat flux differences (Figs. 9 and 10) for daytime, particularly 9 LST to 15 LST, with regions of higher temperatures in GEM_WR compared to GEM_REF collocated with regions of lower (higher) latent (sensible) heat flux and vice versa. The reduced latent and sensible heat fluxes in GEM_WR compared to GEM_REF could be due to the reduced energy at the surface in GEM_WR, given reduced net shortwave radiation. Changes in latent heat fluxes could also be due to differences in the local wind patterns and available soil moisture, which are indirect effects of increased albedo. These are explored in that order below.

To understand better the differences in local/non-synoptic wind patterns such as sea/land breeze, differences in land-water surface temperature gradients between GEM_WR and GEM_REF are analyzed (Fig. 11a). Figure shows that the positive land-water temperature gradients during daytime that drive the sea-breeze type winds are weak in GEM_WR compared to GEM_REF due to the cooler temperatures over land in GEM_WR. This is reflected in Fig. 11b, where the differences in surface (10 m) winds during daytime suggests weaker surface winds over most of Montreal in GEM_WR, except for the eastern region of the island, which matches the latent heat flux differences during daytime, clearly demonstrating that the temperature differences for the non-urban fractions are partly associated with changes in local wind patterns.

The second mechanism for latent heat flux differences, i.e., soil moisture availability, depends on precipitation differences. Comparison of the mean summer precipitation between the two simulations (Fig. 12; top panel) suggests reduced precipitation in GEM_WR, which could lead to reduced soil moisture for non-urban fractions, and therefore latent heat flux. Precipitation decreases by >20 % between 16 and 17 LST, and peak precipitation timing shifts to 19 LST, suggesting a weakened and delayed convective response compared to GEM_REF. This can be explained by the lower daytime temperature and weakened sea breeze, which together weaken the thermodynamic conditions for convective storm development later in the day in GEM_WR, leading to reduced precipitation. The reduced sensible heat flux in GEM_WR during daytime and associated weakening of thermal updrafts that drive boundary layer growth leads to lower PBL height compared to GEM_REF (Fig. 13). The weakened sea breeze further amplifies this effect by limiting moisture transport, convergence, and vertical mixing. Over the island of Montreal, a negative velocity potential and surface wind divergence are noticed in GEM_WR in comparison to GEM_REF, indicating inhibition of rising motion and therefore lowering of convective activity over Montreal (Fig. S3). The velocity potential is estimated using the inverse Laplacian of the wind divergence, which is $\chi=\nabla^{-2}\delta$. Over the nearby water body, anomalous surface wind convergence and a positive velocity potential anomaly are seen, especially during 15–21 LST. This pattern suggests reduced moisture transport from water to land.

As for nighttime, increases in local winds are noted over the island in GEM_WR (Fig. 11b), which can mostly be attributed to increases in land breeze associated with the enhanced negative land-water temperature

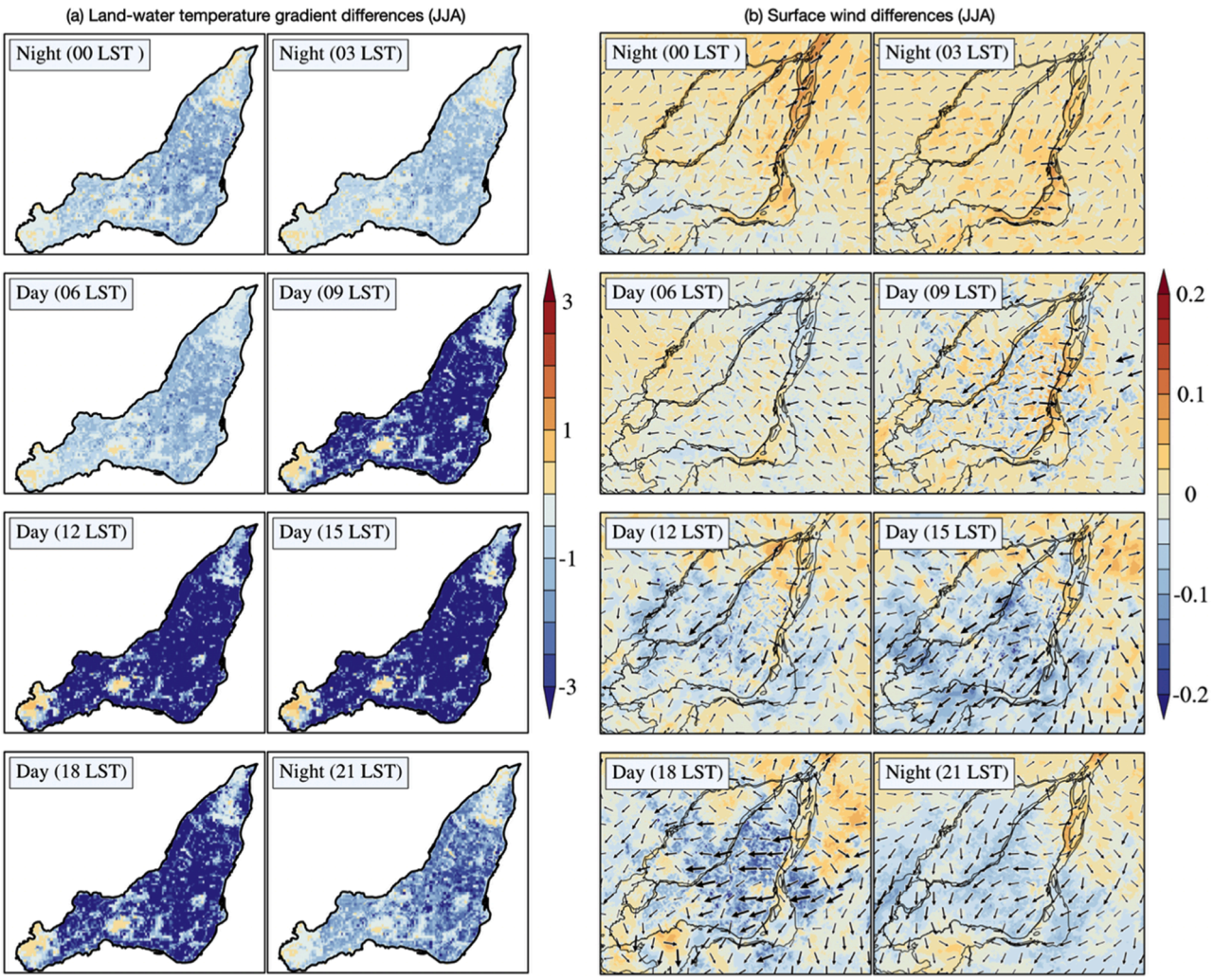

Fig. 11. Differences between GEM_WR and GEM_REF simulated (a) mean summer land-water surface temperature differences (°C) and (b) surface winds (at 10 m, in ms^{-1}).

gradient (Fig. 11a), particularly for 00 LST and 03 LST. The role of non-urban to urban circulation, particularly over the island, is considerably reduced by the weak UHI in GEM_WR (Fig. S4).

The response of non-urban fractions to the enhanced land breeze varies over the island depending on its nearness to the core urban region. Accordingly, the non-urban fractions within the core urban region (i.e., the south-central part of the island), which are considerably smaller than the urban fractions, experience cooler temperatures in GEM_WR (Fig. 8b) due to the stronger land breeze for these regions that removes the residual warm air through horizontal advection as it moves toward the adjacent, relatively warmer, water body. The non-urban fractions outside the core urban region, and in the path of the land breeze, on the other hand, experience warming due to the advection of warmer temperatures from the core urban region.

Fig. 14 illustrates a schematic representation of the main impacts of the cooling strategy on urban climate. It indicates that the expected cooling potential of white roofs may not be fully achievable for the island of Montreal due to the complex interactions discussed above. It is worth noting that the identification of non-urban fractions with warmer temperatures in GEM_WR compared to GEM_REF is useful in that additional strategies can be considered to further mitigate heat impacts.

4. Discussion and conclusions

This study quantifies the impact of white roofs, used as an urban heat mitigation strategy, including its broader effects on local climate dynamics for the Montreal island by utilizing super-resolution regional climate model simulations, with and without white roof implementation, i.e. GEM_WR and GEM_REF. The main findings are summarized below.

- The validation of model simulated temperature, precipitation and wind characteristics against observation suggests reasonably good performance of the model. The observed wind roses demonstrate the existence of non-synoptic wind patterns such as land and sea breezes for the shoreline regions of Montreal island, even though they are less pronounced compared to oceanic settings. The 250 m super-resolution GEM simulations capture these wind patterns, albeit with some differences in direction and magnitude compared to observations.
- The higher roof albedo in GEM_WR, representative of white roof implementation, yields lower grid-averaged temperatures over Montreal compared to GEM_REF. However, analysis of the urban and non-urban fractions for different hours of the day shows overall cooling for urban fractions, while both cooling and warming are noted for non-urban fractions, due to the complex interactions between various aspects of the regional climate system. The cooling/warming for non-urban fractions are significantly lower in magnitude compared to the cooling for urban fractions.

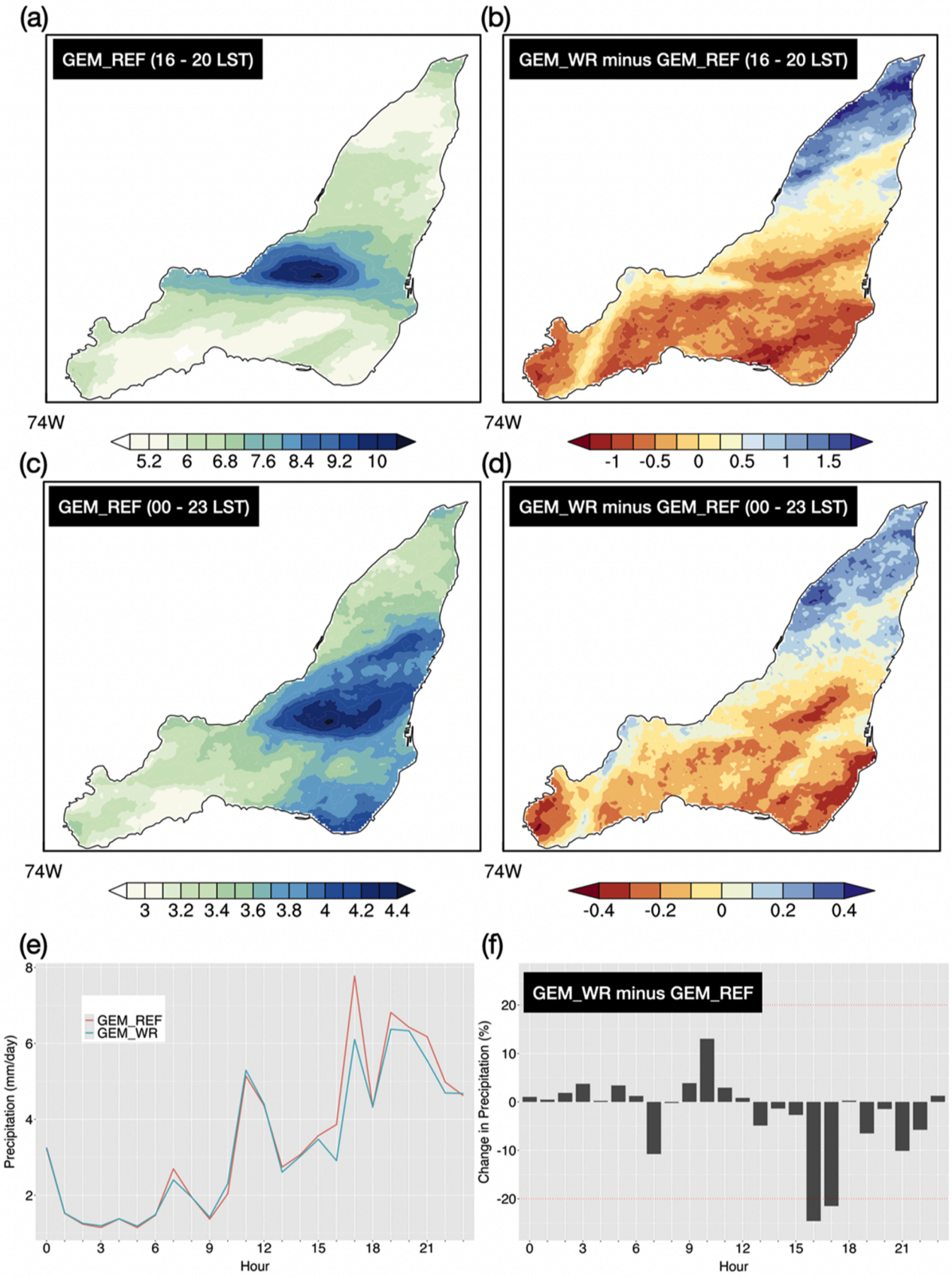

Fig. 12. (a) Mean summer precipitation (mm/day) for the 16–20 LST period over Montreal Island based on GEM_REF. (b) Differences between GEM_WR and GEM_REF for the same period. (c) and (d) are the same as (a) and (b), respectively, but for mean summer precipitation. (e) Diurnal variation of precipitation over Montreal from GEM_REF and GEM_WR. (f) Percentage difference in precipitation between GEM_WR and GEM_REF.

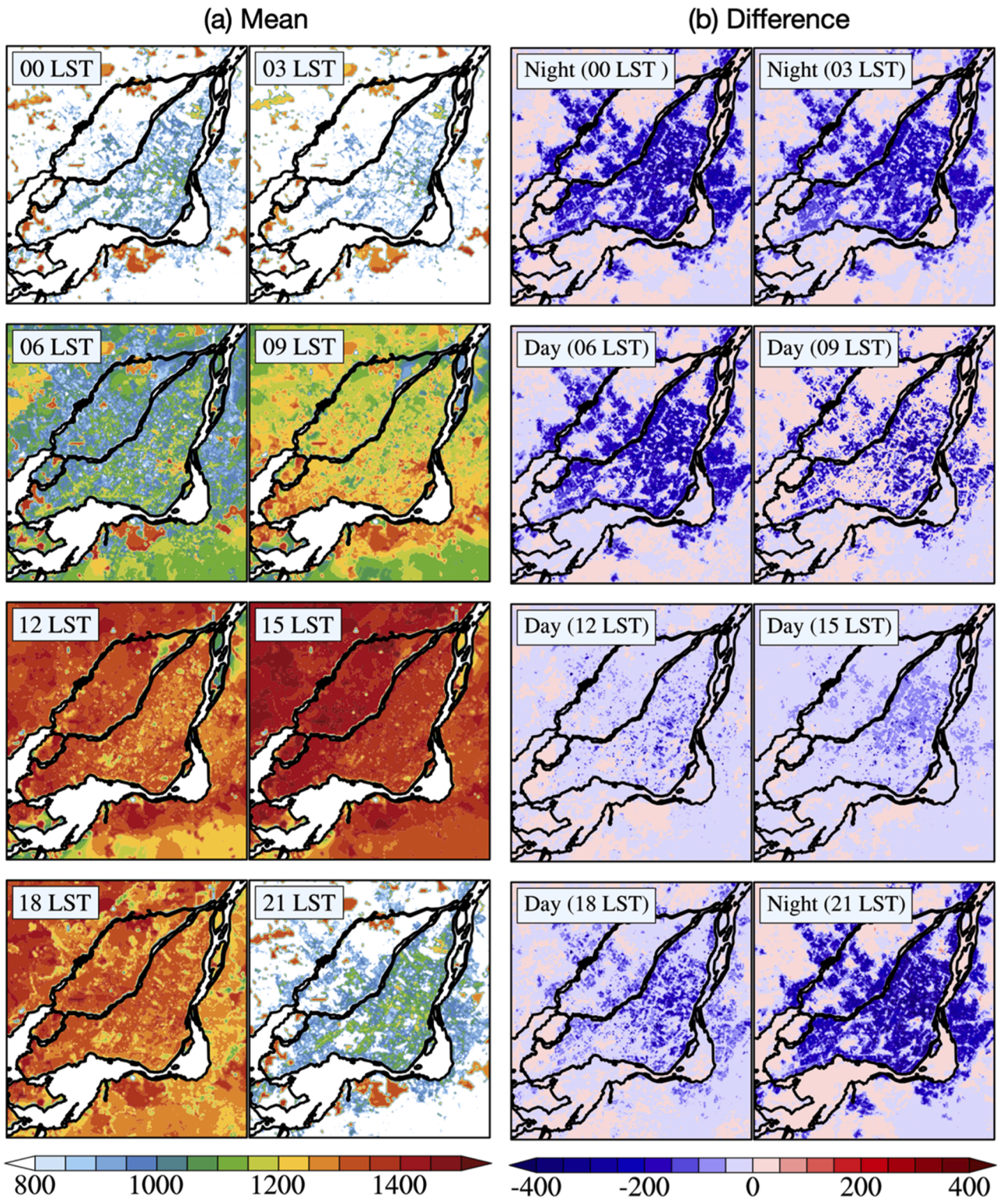

Fig. 13. (a) Mean summer planetary boundary layer height (m) in GEM_REF. (b) PBL height differences between GEM_WR and GEM_REF.

- Daytime warming noted for non-urban fractions is linked to reduced latent heat flux, which results from reduced surface energy, weakening of sea breeze circulation, and decreased soil moisture from reduced convective precipitation.
- Nighttime warming noted for the non-urban fractions within the low-density urban zones can be attributed to the advection of relatively warmer air from nearby urban regions via enhanced land breeze directed toward the adjacent water body in GEM_WR.
- While reflective roofing mitigates heat stress over the study region, localized warming in non-urban fractions raises potential social equity concerns. The differential cooling/warming results for urban/non-urban fractions highlight the need for additional mitigation strategies to avoid negative impacts from the large-scale implementation of white roofs for non-urban fractions and to meet cooling needs.

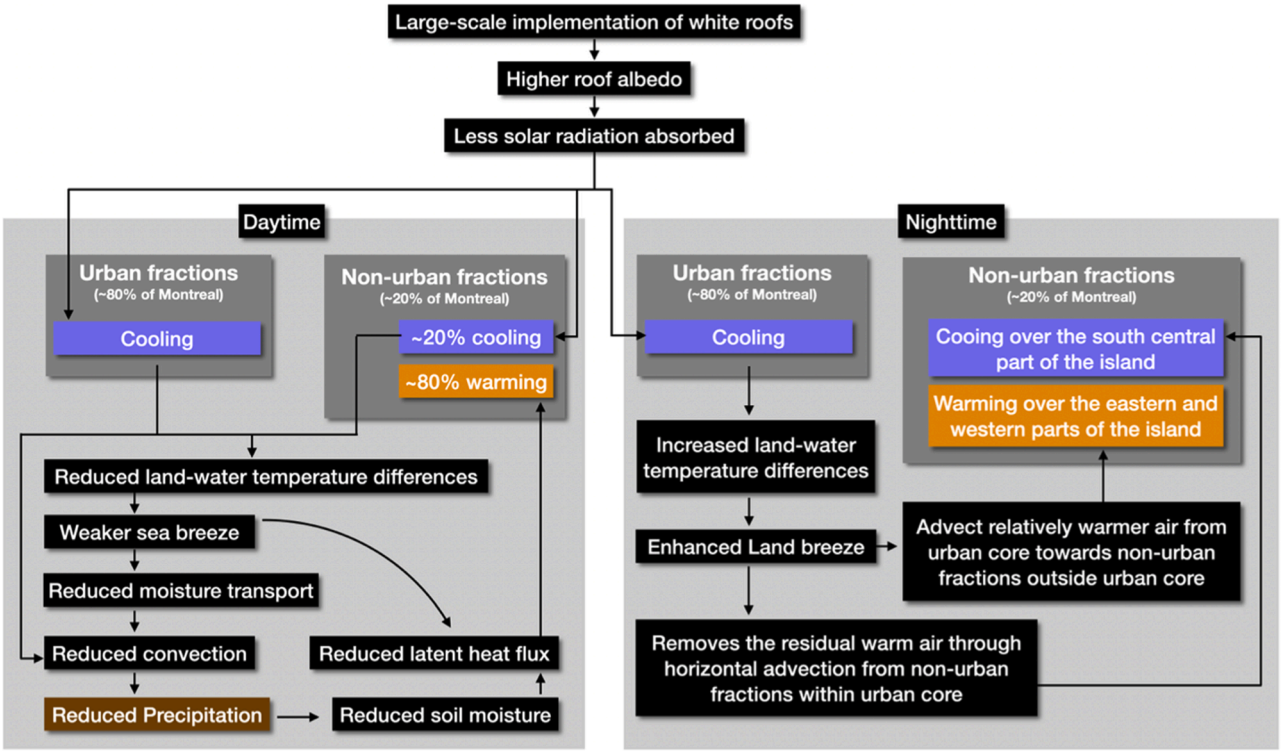

Fig. 14. Schematic representation illustrating net impact of white roofs on the urban climate, considering also changes to local wind patterns.

This research underscores the importance of integrated urban planning that considers the interactions between land surface modifications and atmospheric processes. The application of super-resolution climate modelling that incorporates TEB scheme goes beyond assessing the net cooling benefits of white roofs. It emphasizes the significance of this modelling framework in capturing local wind dynamics and their varying effects on urban and non-urban fractions. Understating of the varied response of urban and non-urban regions is important in guiding implementation of UHI reduction techniques, which may be even more important in the future climate.

Future studies can focus on increasing model resolution to further enhance the realism of the simulations, given that all urban regions, as well as non-urban regions, for a model grid cell are treated as though they are juxtaposed. Although this study quantifies the meteorological impacts of large-scale white roof implementation, it does not explicitly assess potential implications such as those related to building energy demand or human health outcomes.

Previous research has shown that the white roof albedo effects vary greatly by season and latitude. The benefits of improving roof albedo are limited or even negated at high latitudes during the winter months due to decreased solar insolation, high snow reflection, and increased heating demand [51]. A recent study by Macintyre et al. [52] has shown that reflective roofs can substantially reduce summertime heat exposure and associated mortality, while their wintertime effects are generally negligible or even offset by the supportive role of the winter UHI. These findings suggest that although present study does not quantify health outcomes, large-scale white roof implementation is likely to yield net public health benefits, particularly during summer months. In this study, only two summer years were considered due to computational limitations, and the results may be influenced by interannual variability in local circulations and associated precipitation and heat extremes. Therefore, seasonal and long-term monitoring and modeling to better understand the implications of urban heat mitigation strategies is indispensable.

Roof albedo/reflectivity varies over time due to gradual implementation and material degradation amongst other factors and long-term simulations spanning several years should take this into consideration. Similarly, future research should look at intermediate and more realistic albedo values to properly quantify implications over Montreal that are important to policy. Furthermore, experiments using white roofs with other cooling approaches (e.g., urban forests, green roofs, and high-albedo pavements) could facilitate identification of synergistic impacts and benefits.

CRediT authorship contribution statement

Shinto Roose: Writing – original draft, Visualization, Validation, Methodology, Investigation, Formal analysis, Conceptualization. **Laxmi Sushama:** Writing – review & editing, Supervision, Resources, Methodology, Investigation, Funding acquisition, Conceptualization.

Declaration of competing interest

Authors have no competing financial and/or non-financial interests.

Acknowledgement

This research was funded by the Natural Sciences and Engineering Research Council of Canada, Trottier Institute for Sustainability in Engineering and Design, and Bieler School of Environment. The GEM simulations considered in this study were performed on the supercomputer managed by the Digital Research Alliance of Canada and Calcul Québec.

Supplementary materials

Supplementary material associated with this article can be found, in the online version, at doi:10.1016/j.rineng.2025.107572.

Data availability

Data will be made available on request.

References

[1] IPCC, Summary for Policymakers, in: P.R. Shukla, J. Skea, A. Reisinger, R. Slade, R. Fradera, M. Pathak, A. Al Khourdajie, M. Belkacemi, R. van Diemen, A. Hasija, G. Lisboa, S. Luz, J. Malley, D. McCollum, S. Some, P. Vyas, P.R. Shukla, J. Skea, R. Slade, A. Al Khourdajie, R. van Diemen, D. McCollum, M. Pathak, S. Some, P. Vyas, R. Fradera, M. Belkacemi, A. Hasija, G. Lisboa, S. Luz, J. Malley (Eds.), Climate Change 2022: Mitigation of Climate Change. Contribution of Working Group III to the Sixth Assessment Report of the Intergovernmental Panel On Climate Change, Cambridge University Press, Cambridge, UK and New York, NY, USA, 2022, https://doi.org/10.1017/9781009157926.001.

[2] IPCC, Annex II: glossary, in: V. Möller, R. van Diemen, J.B.R. Matthews, C. Méndez, S. Semenov, J.S. Fuglestvedt, A. Reisinger, H.-O. Pörtner, D.C. Roberts, M. Tignor, E.S. Poloczanska, K. Mintenbeck, A. Alegría, M. Craig, S. Langsdorf, S. Löschke, V. Möller, A. Okem, B. Rama (Eds.), *Climate Change* 2022: *Impacts, Adaptation and Vulnerability. Contribution of Working Group II to the Sixth Assessment Report of the Intergovernmental Panel On Climate Change*, Cambridge University Press, Cambridge, UK and New York, NY, USA, 2022, pp. 2897–2930, https://doi.org/10.1017/9781009325844.029.

[3] F. Roberge, L. Sushama, Urban heat island in current and future climates for the island of Montreal, Sustain. Cities Soc. 40 (2018) 501–512, https://doi.org/10.1016/j.scs.2018.04.033.

[4] B.G. Nancy, et al., Global Change and the Ecology of Cities, Science 319 (2008) 756–760, https://doi.org/10.1126/science.1150195.

[5] D. Dodman, B. Hayward, M. Pelling, V. Castan Broto, W. Chow, E. Chu, R. Dawson, L. Khirfan, T. McPhearson, A. Prakash, Y. Zheng, G. Ziervogel, Cities, Settlements and Key Infrastructure, in: H.-O. Pörtner, D.C. Roberts, M. Tignor, E. S. Poloczanska, K. Mintenbeck, A. Alegría, M. Craig, S. Langsdorf, S. Löschke, V. Möller, A. Okem, B. Rama (Eds.), *Climate Change 2022: Impacts, Adaptation and Vulnerability*. Contribution of Working Group II to the Sixth Assessment Report of the Intergovernmental Panel On Climate Change, Cambridge University Press, Cambridge, UK and New York, NY, USA, 2022, pp. 907–1040, https://doi.org/10.1017/9781009325844.008.

[6] United Nations, World Population Prospects 2019: Highlights, 2019. https://population.un.org/wpp/Publications/Files/WPP2019_Highlights.pdf.

[7] J. Feng, K. Gao, H. Khan, G. Ulpiani, K. Vasilakopoulou, G. Young Yun, M. Santamouris, Overheating of cities: magnitude, characteristics, impact, mitigation and adaptation, and future challenges, Annu. Rev. Environ. Resour. 48 (2023) 651–679, https://doi.org/10.1146/annurev-environ-112321-093021.

[8] A.J. Arnfield, Two decades of urban climate research: a review of turbulence, exchanges of energy and water, and the urban heat island, Int. J. Climatol. 23 (2003) 1–26, https://doi.org/10.1002/joc.859.

[9] H. Li, Y. Zhou, X. Wang, X. Zhou, H. Zhang, S. Sodoudi, Quantifying urban heat island intensity and its physical mechanism using WRF/UCM, Sci. Total Environ. 650 (2019) 3110–3119, https://doi.org/10.1016/j.scitotenv.2018.10.025.

[10] Y. Li, S. Schubert, J.P. Kropp, et al., On the influence of density and morphology on the Urban Heat Island intensity, Nat. Commun. 11 (2020) 2647, https://doi.org/10.1038/s41467-020-16461-9.

[11] L.W.A. Van Hove, C.M.J. Jacobs, B.G. Heusinkveld, J.A. Elbers, B.L. van Driel, A.A. M Holtslag, Temporal and spatial variability of urban heat island and thermal comfort within the Rotterdam agglomeration, Build. Environ. 83 (2015) 91–103, https://doi.org/10.1016/j.buildenv.2014.08.029.

[12] J. Abu Qadourah, Energy efficiency evaluation of green roofs as a passive strategy in the mediterranean climate, Results Eng. 23 (2024) 102519, https://doi.org/10.1016/j.rineng.2024.102519.

[13] A. Aflaki, M. Mirnezhad, A. Ghaffarianhoseini, A. Ghaffarianhoseini, H. Omrany, Z. H. Wang, H. Akbari, Urban heat island mitigation strategies: a state-of-the-art review on Kuala Lumpur, Singapore and Hong Kong, Cities 62 (2017) 131–145, https://doi.org/10.1016/j.cities.2016.09.003.

[14] A.A. Kafy, K.A. Crews, A.E. Thompson, Exploring the cooling potential of green roofs for mitigating diurnal heat island intensity by utilizing Lidar and Artificial Neural Network, Sustain. Cities Soc. 116 (2024) 105893, https://doi.org/10.1016/j.scs.2024.105893.

[15] E.M. Khotbehsara, A.B. Daemei, F.A. Malekjahan, Simulation study of the eco green roof in order to reduce heat transfer in four different climatic zones, Results Eng. 2 (2019) 100010, https://doi.org/10.1016/j.rineng.2019.100010.

[16] P. Kumar, S.E. Debele, S. Khalili, C.H. Halios, J. Sahani, N. Aghamohammadi, M. de Fatima Andrade, M. Athanassiadou, K. Bhui, N. Calvillo, S.-J. Cao, F. Coulon, J. L. Edmondson, D. Fletcher, E. Dias de Freitas, H. Guo, M.C. Hort, M. Katti, T. R. Kjeldsen, L. Jones, Urban heat mitigation by green and blue infrastructure: drivers, effectiveness, and future needs, Innovation 5 (2) (2024) 100588, https://doi.org/10.1016/j.xinn.2024.100588.

[17] K. McConnell, C.V. Braneon, E. Glenn, N. Stamler, E. Mallen, D.P. Johnson, C. Rosenzweig, A quasi-experimental approach for evaluating the heat mitigation effects of green roofs in Chicago, Illinois, Sustain. Cities Soc. 76 (2022) 103376, https://doi.org/10.1016/j.scs.2021.103376.

[18] A. Synnefa, T. Karlessi, N. Gaitani, M. Santamouris, D.N. Assimakopoulos, C. Papakatsikas, Experimental testing of cool colored thin layer asphalt and estimation of its potential to improve the urban microclimate, Build. Environ. 46 (1) (2011) 38–44, https://doi.org/10.1016/j.buildenv.2010.06.014. Scopus.

[19] A. Baniassadi, D.J. Sailor, G.A. Ban-Weiss, Potential energy and climate benefits of super-cool materials as a rooftop strategy, Urban Climate 29 (2019) 100495, https://doi.org/10.1016/j.uclim.2019.100495.

[20] M.H. Elnabawi, N. Hamza, R. &Raveendran, Super cool roofs': mitigating the UHI effect and enhancing urban thermal comfort with high albedo-coated roofs, Results Eng. 19 (101269) (2023) 101269, https://doi.org/10.1016/j.rineng.2023.101269.

[21] J. Feng, A. Khan, Q.-V. Doan, K. Gao, M. Santamouris, The heat mitigation potential and climatic impact of super-cool broadband radiative coolers on a city scale, Cell Rep. Phys. Sci. 2 (7) (2021) 100485, https://doi.org/10.1016/j.xcrp.2021.100485.

[22] S. Garshasbi, J. Feng, R. Paolini, J. Jonathan Duverge, C. Bartesaghi-Koc, S. Arasteh, A. Khan, M. Santamaria, On the energy impact of cool roofs in Australia, Energy Build. 278 (2023) 112577, https://doi.org/10.1016/j.enbuild.2022.112577.

[23] X. Lim, The super-cool materials that send heat to space, Nature 577 (7788) (2019) 18–21, https://doi.org/10.1038/d41586-019-03911-8.

[24] A. Mohammed, A. Khan, M. Santamaria, Numerical evaluation of enhanced green infrastructures for mitigating urban heat in a desert urban setting, Build. Simul. (2022), https://doi.org/10.1007/s12273-022-0940-x.

[25] M. Santamouris, G.Y. Yun, Recent development and research priorities on cool and super cool materials to mitigate urban heat island, Renew. Energy 161 (2020) 792–807, https://doi.org/10.1016/j.renene.2020.07.109.

[26] Y. Sun, B. Fang, K.W. Oleson, L. Zhao, D.O. Topping, D.M. Schultz, Z. Zheng, Improving urban climate adaptation modeling in the community earth system model (CESM) through transient urban surface albedo representation, J. Adv. Model. Earth Syst. 16 (12) (2024) e2024MS004380.

[27] L. Wang, M. Huang, D. Li, Where are white roofs more effective in cooling the surface? Geophys. Res. Lett. 47 (2020) e2020GL087853 https://doi.org/10.1029/2020GL087853.

[28] N. Kaloustian, H. Bitar, Y. Diab, Urban heat island and urban planning in Beirut, Procedia Eng. 169 (2016) 72–79.

[29] R. Hamdi, V. Masson, Inclusion of a Drag Approach in the Town Energy Balance (TEB) Scheme: offline 1D Evaluation in a Street Canyon, J. Appl. Meteor. Climatol. 47 (2008) 2627–2644, https://doi.org/10.1175/2008JAMC1865.1.

[30] A. Lemonsu, V. Viguie, M. Daniel, V. Masson, Vulnerability to heat waves: impact of urban expansion scenarios on urban heat island and heat stress in Paris (France), Urban Climate 14 (2015) 586–605.

[31] B. Teufel, L. Sushama, V. Poitras, T. Dukhan, S. Bélair, L. Miranda-Moreno, L. Sun, A.P. Sasmito, G. Bitsuamlak, Impact of COVID-19-Related Traffic Slowdown on Urban Heat Characteristics, Atmosphere 12 (2) (2021) 243, https://doi.org/10.3390/atmos12020243.

[32] S. Afroditi, Chapter 6 - the impact of heat mitigation on energy demand, in: N. Aghamohammadi, M. Santamouris (Eds.), Mitigation and Adaptation of Urban Overheating, Elsevier, 2024, pp. 175–211, https://doi.org/10.1016/B978-0-443-13502-6.00006-3.

[33] O. Brousse, C. Simpson, A. Zonato, A. Martilli, J. Taylor, M. Davies, C. Heaviside, Cool roofs could be most effective at reducing outdoor urban temperatures in London (United Kingdom) compared with other roof top and vegetation interventions: a mesoscale urban climate modeling study, Geophys. Res. Lett. 51 (2024) e2024GL109634, https://doi.org/10.1029/2024GL109634.

[34] A. Khan, L. Carlosena, S. Khorat, et al., Urban cooling potential and cost comparison of heat mitigation techniques for their impact on the lower atmosphere, Comput.Urban Sci. 3 (2023) 26, https://doi.org/10.1007/s43762-023-00101-1.

[35] P. Patel, S. Karmakar, S. Ghosh, D.G. Aliaga, D. Niyogi, Impact of green roofs on heavy rainfall in tropical, coastal urban area, Environ. Res. Lett. 16 (7) (2021) 074051, https://doi.org/10.1088/1748-9326/ac1011.

[36] J. Song, Z.-H. Wang, C. Wang, The regional impact of urban heat mitigation strategies on planetary boundary layer dynamics over a semiarid city, J. Geophys. Res. Atmos. 123 (12) (2018) 6410–6422, https://doi.org/10.1029/2018JD028302.

[37] J. Côté, S. Gravel, A. Méthot, A. Patoine, M. Roch, A. Staniforth, The operational cmc–mrb global environmental multiscale (gem) model. part i: design considerations and formulation, Mon. Weather Rev. 126 (6) (1998) 1373–1395, https://doi.org/10.1175/1520-0493(1998)126⟨1373:TOCMGE⟩2.0.CO;2.

[38] H. Hersbach, B. Bell, P. Berrisford, S. Hirahara, A. Horányi, J. Muñoz-Sabater, J. Nicolas, C. Peubey, R. Radu, D. Schepers, A. Simmons, C. Soci, S. Abdalla, X. Abellan, G. Balsamo, P. Bechtold, G. Biavati, J. Bidlot, M. Bonavita, J.-N. Thépaut, The ERA5 global reanalysis, Quart. J. Roy. Meteorol. Soc. 146 (730) (2020) 1999–2049, https://doi.org/10.1002/qj.3803.

[39] J.A. Milbrandt, M.K. Yau, A multimoment bulk microphysics parameterization. part i: analysis of the role of the spectral shape parameter, J. Atmos. Sci. 62 (9) (2005) 3051–3064, https://doi.org/10.1175/JAS3534.1.

[40] J. Li, H.W. Barker, A radiation algorithm with correlated-k distribution. part i: local thermal equilibrium, J. Atmos. Sci. 62 (2) (2005) 286–309, https://doi.org/10.1175/JAS-3396.1.

[41] R. Benoit, J. Côté, J. Mailhot, Inclusion of a tke boundary layer parameterization in the canadian regional finite-element model, Mon. Weather Rev. 117 (8) (1989) 1726–1750, https://doi.org/10.1175/1520-0493(1989)117⟨1726:IOATBL⟩2.0.CO;2.

[42] Y. Delage, Parameterising sub-grid scale vertical transport in atmospheric models under statically stable conditions, Boundary Layer Meteorol. 82 (1) (1997) 23–48, https://doi.org/10.1023/A:1000132524077.

[43] A. Zadra, R. McTaggart-Cowan, R. Michel, Recent changes to the orographic blocking. Seminar Presentation, RPN, Dorval, Canada, 2012, 30 March 2012. [Accessed: 2023-09-20], https://collaboration.cmc.ec.gc.ca/science/rpn/SEM/dossiers/2012/seminaires/2012-0330/Seminar-2012-03-30-Ayrton-Zadra.pdf.

[44] G.T. Diro, L. Sushama, Simulating Canadian arctic climate at convection-permitting resolution, Atmosphere 10 (8) (2019), https://doi.org/10.3390/atmos10080430.

[45] Verseghy, D. (2009). *CLASS—The Canadian land surface scheme (version 3.4)—Technical documentation (version 1.1)* (tech. rep.). Internal report, Climate Research Division, Science and Technology Branch, Environment Canada.
[46] V. Masson, A Physically-Based scheme for the urban energy budget in atmospheric models, Boundary Layer Meteorol. 94 (3) (2000) 357–397.
[47] M.M. Thornton, R. Shrestha, Y. Wei, P.E. Thornton, S.-C. Kao, Daymet: Station-Level Inputs and Cross-Validation for North America, Version 4 R1, ORNL DAAC, Oak Ridge, Tennessee, USA, 2022, https://doi.org/10.3334/ORNLDAAC/2132.
[48] J. Muñoz-Sabater, E. Dutra, A. Agustí-Panareda, C. Albergel, G. Arduini, G. Balsamo, S. Boussetta, M. Choulga, S. Harrigan, H. Hersbach, B. Martens, D. G. Miralles, M. Piles, N.J. Rodríguez-Fernández, E. Zsoter, C. Buontempo, J.-N. Thépaut, ERA5-Land: a state-of-the-art global reanalysis dataset for land applications, Earth Syst. Sci. Data 13 (2021) 4349–4383, https://doi.org/10.5194/essd-13-4349-2021.
[49] Kindstedt, I., Schild, K., Winski, D., Kreutz, K., Copland, L., Campbell, S., & McConnell, E. (2021). Evaluating Sources of an Apparent Cold Bias in MODIS Land Surface Temperatures in the St. Elias Mountains, Yukon, Canada. doi:10.5194/tc-2021-211.
[50] A. Vincent, L. Sushama, City-scale modelling of road thermal and hydrologic characteristics and failure mechanisms: Case study of Montreal, Sustainable Cities and Society 108 (2024) 105484, https://doi.org/10.1016/j.scs.2024.105484.
[51] K.W. Oleson, G.B. Bonan, J. Feddema, Effects of white roofs on urban temperature in a global climate model, Geophys. Res. Lett. 37 (3) (2010).
[52] H.L. Macintyre, C. Heaviside, X. Cai, R. Phalkey, Comparing temperature-related mortality impacts of cool roofs in winter and summer in a highly urbanized European region for present and future climate, Environ. Int. 154 (2021) 106606.